



Article

A Novel Crossbeam Structure with Graphene Sensing Element for N/MEMS Mechanical Sensors

Junqiang Wang^{1,2,*} , Zehua Zhu^{1,2}, Yue Qi^{1,2} and Mengwei Li^{1,2,*}

¹ National Key Laboratory of Instrumentation Science & Dynamic Measurement, North University of China, Taiyuan 030051, China; zehua_zhu@163.com (Z.Z.); qiyuenuc@163.com (Y.Q.)

² Academy for Advanced Interdisciplinary Research, North University of China, Taiyuan 030051, China

* Correspondence: wangjq210@nuc.edu.cn (J.W.); lmwnuc@163.com (M.L.); Tel.: +86-158-1133-8056 (J.W.); +86-139-3424-8366 (M.L.)

Abstract: A graphene membrane acts as a highly sensitive element in a nano/micro–electro–mechanical system (N/MEMS) due to its unique physical and chemical properties. Here, a novel crossbeam structure with a graphene varistor protected by Si₃N₄ is presented for N/MEMS mechanical sensors. It substantially overcomes the poor reliability of previous sensors with suspended graphene and exhibits excellent mechano-electrical coupling performance, as graphene is placed on the root of the crossbeam. By performing basic mechanical electrical measurements, a preferable gauge factor of ~1.35 is obtained. The sensitivity of the graphene pressure sensor based on the crossbeam structure chip is 33.13 mV/V/MPa in a wide range of 0~20 MPa. Other static specifications, including hysteresis error, nonlinear error, and repeatability error, are 2.0119%, 3.3622%, and 4.0271%, respectively. We conclude that a crossbeam structure with a graphene sensing element can be an application for the N/MEMS mechanical sensor.

Keywords: graphene; N/MEMS; displacement sensor; pressure sensor



Citation: Wang, J.; Zhu, Z.; Qi, Y.; Li, M. A Novel Crossbeam Structure with Graphene Sensing Element for N/MEMS Mechanical Sensors. *Nanomaterials* **2022**, *12*, 2101. <https://doi.org/10.3390/nano12122101>

Academic Editor: Filippo Giannazzo

Received: 16 May 2022

Accepted: 16 June 2022

Published: 18 June 2022

Publisher's Note: MDPI stays neutral with regard to jurisdictional claims in published maps and institutional affiliations.



Copyright: © 2022 by the authors. Licensee MDPI, Basel, Switzerland. This article is an open access article distributed under the terms and conditions of the Creative Commons Attribution (CC BY) license (<https://creativecommons.org/licenses/by/4.0/>).

1. Introduction

Graphene, a two-dimensional material, has excellent mechanical, thermal, optical, and electrical properties. With its Young's modulus of up to 1 TPa [1], thermal conductivity reaching 5×10^3 W/m·K [2], light transmittance as high as 97.7% [3], and an ultrahigh carrier mobility of $200,000 \text{ cm}^2 \cdot \text{V}^{-1} \cdot \text{s}^{-1}$ [4], it has become the preferred material for the sensing element in various sensors. Moreover, graphene will be suitable for MEMS and NMES mechanical sensors in the future due to two primary factors: the piezoresistive effect because of graphene microstructure changing under external stress and high compatibility between graphene transferring patterning and micro–nano process technology [5,6].

In previous research, graphene sensors have been used to detect multiple different mechanical parameters, such as pressure [7,8], acceleration, and strain [9–12]. The first typical graphene pressure sensor was proposed by Smith et al. [13,14]. A monolayer graphene membrane was suspended on a cavity in SiO₂/Si substrate, and a sensitivity of $3.95 \mu\text{V}/\text{V}/\text{mmHg}$ was obtained as pressure ranged from 200 to 1000 mbar. There is also an unfavorable phenomenon where liquid remains in the square cavity during the graphene wet transferring process. Subsequently, the electrical property of graphene is inevitably affected, which leads to poor stability of the suspended graphene pressure sensor. A new type of graphene pressure sensor was developed by Zhu et al. [15]. A folded graphene ribbon was placed on the maximum strain region of a suspended square Si₃N₄ film, and sensitivity reached up to 8.5 mV/bar with pressure ranging from 0 to 700 mbar. In addition, a more sensitive graphene pressure sensor was developed by Wang et al. [8]. Suspended Si₃N₄ for supporting graphene was etched to form substantial numbers of through hole arrays. Owing to the increased strain on the graphene membrane, the pressure sensor showed a sensitivity of $2.8 \times 10^{-5} \text{ mbar}^{-1}$ under a pressure of 0~400 mbar.

Although residual liquid in the cavity can be resolved by the suspended Si_3N_4 approach, the measurement range is below 1 MPa due to the process limitations of the suspended Si_3N_4 structure. In the past few years, some researchers have also made great progress in graphene based accelerometers. A suspended graphene high-g accelerometer made by Hurst et al. has a high repeatable response to a wide range of 1000~3000 g [16]. Another NMES accelerometer with a suspended double layer graphene ribbon with attached silicon proof mass was fabricated by Fan et al. and could measure an effective acceleration of 20~30 g [10]. These suspended graphene mechanical sensors are simple in structure and exhibit excellent electrical performance. Structural stability and reliability, however, require further improvement. For example, suspended graphene is prone to collapse and rupture [17], and an ultra-thin graphene beam has high processing difficulty and low natural frequency. A crossbeam structure, with its excellent mechanical properties, is commonly used in large impact and high-load environments [18,19]. In addition, the sensitivity of graphene mechanical sensors is related to the effect of stress or strain on the sensing element. Compared with the ordinary ribbon of graphene, the fold pattern can capture multiple responses and improve the detection capability of a sensor.

As the core element of a pressure sensor, the quality of graphene directly affects the piezoresistive performance of the device. Improper operation during the graphene transferring process can easily introduce some defects and residues, such as wrinkling, cracking, and photoresistance [20]. This can cause a risk of Dirac point shift and lead to poor resistivity stability [21–23]. Combined annealing for van der Waals force enhancement and water bath heating for cleaning, the performance of graphene can be effectively improved. Another concern is that covering suspended graphene with a passivation layer becomes more difficult. When graphene is exposed to air during fabrication or employment, it is easily contaminated by gas adsorption (e.g., N_2 , O_2 , CO_2 , H_2O , etc.) or other impurities, causing n-/p-type doping in graphene [24,25]. As a result, graphene resistance sharply changes, sensor reliability shows large decreases, and serving life noticeably shortens [26]. Generally, materials with a strong affinity, such as polymer, h-BN, Al_2O_3 , and Si_3N_4 , are used to protect the graphene sensing element and can improve the electrical properties and long-term stability of sensors [27–32]. Compared with Al_2O_3 , depositing and etching Si_3N_4 are relatively convenient methods [33,34], and Si_3N_4 processing is also highly compatible with N/MEMS technology, avoiding risk of oxidation under high temperature [35–37]. Additionally, it is beneficial for covering Si_3N_4 , rather than organic polymer or h-BN, on graphene to reduce organic residue pollution in subsequent processing. In this paper, a novel crossbeam structure with a graphene sensing element is presented for N/MEMS mechanical sensors. The core graphene varistors are encapsulated with Si_3N_4 film to achieve highly sensitive pressure detection.

2. Materials and Methods

2.1. Fabrication of N/MEMS Crossbeam Structure

The fabrication process is shown in Figure 1. A passivation layer of Si_3N_4 with a thickness of 200 nm was first deposited on 2" Si wafer by plasma enhanced chemical vapor deposition (PECVD). The electrode, 15 nm/25 nm thick Cr/Au, was followed by magnetron sputtering [Figure 1a]. A square $900 \times 900 \mu\text{m}$ cavity was then created on the back of the wafer by deep reactive ion etching (DRIE) [Figure 1b]. Subsequently, the Si wafer was diced into small $17 \times 17 \text{ mm}$ dies, and the CVD-grown monolayer graphene (TTG, ACS Material, LLC, Pasadena, CA, USA) was transferred and patterned by PMMA assistance and oxygen plasma etching, respectively [Figure 1c]. A thin 150 nm thick Si_3N_4 film was also deposited by PECVD to protect the graphene from undesired doping and pollution in the ambient environment. Reactive ion etching (RIE) was used to remove Si_3N_4 on the Pad, and Cr/Au with a thickness of 25/100 nm was sputtered on the Pad [Figure 1d]. Finally, four square cavities with dimensions of $350 \times 350 \mu\text{m}$ were etched by DRIE to create a crossbeam with a length of $900 \mu\text{m}$, width of $200 \mu\text{m}$, and thickness of $40 \mu\text{m}$ [Figure 1e].

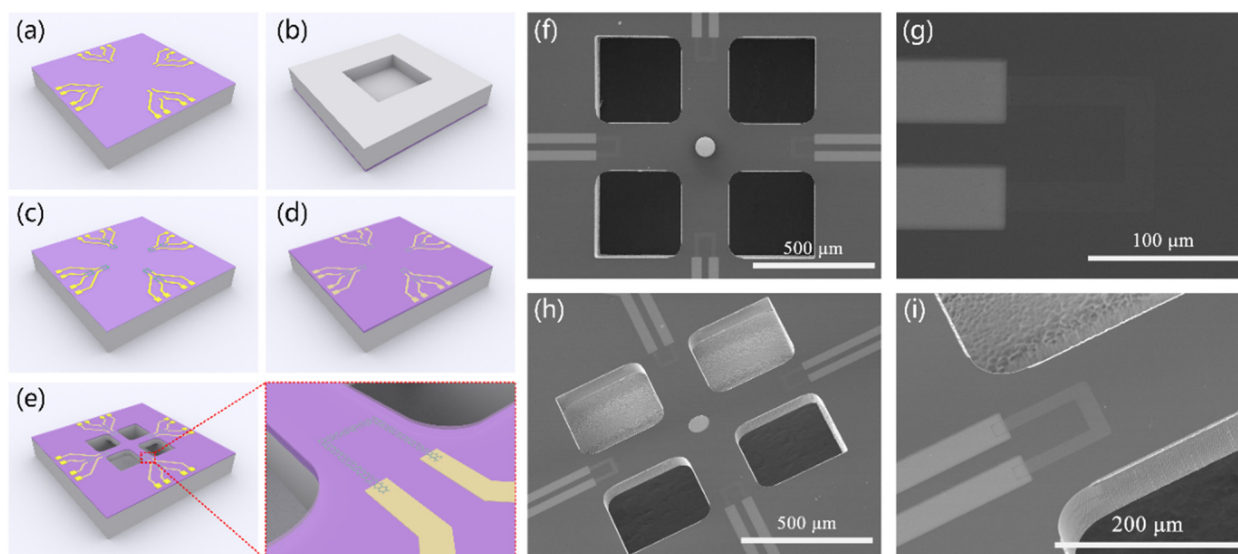


Figure 1. Fabrication process and SEM images of crossbeam structure with graphene sensing element. (a) Sputtering Cr/Au electrode. (b) Etching deep square cavity on the back of wafer. (c) Transferring and patterning monolayer graphene. (d) Depositing protective layer of Si_3N_4 and etching Si_3N_4 to leak out the Pad and sputtering Cr/Au on it. (e) Release crossbeam structure. (f) Top view of whole chip. (g) Top view of single graphene element. (h) Tilt observation of whole chip. (i) Tilt observation of single graphene element.

The crossbeam structure with the graphene sensing element was firstly measured using a scanning electron microscope (Quanta 250, FEI, Inc., Hillsboro, OR, USA). Figure 1f,g shows the top view of the whole chip and single graphene element, respectively. Four identical graphene piezoresistors were arranged at the root of crossbeam. Measurement results of the crossbeam, 900 μm in length and 200 μm in width, confirmed the consistency with the design. The size of the folded graphene ribbon was determined as 30 μm long and 10 μm wide. As shown in Figure 1h,i, the crossbeam structure was also inspected using a SEM with a tilt angle. It is clear that the crossbeam thickness at the root was thicker than that in the middle because of the universal feature of the DRIE process. Nevertheless, it had almost no influence on the mechanical properties of crossbeam.

2.2. Schematic of Transfer Process of Graphene Layer

Single-layer graphene (Gra) was grown on a Cu substrate. After being cropped into a 1.5×1.5 cm sample, we coated the graphene on Cu foil with polymethyl methacrylate (PMMA) using a spin coater at speeds of 600 rpm/5 s and 4000 rpm/30 s. The PMMA/Gra/Cu/Gra sample was placed on a hot plate at 130 $^\circ\text{C}$ for 20 min. Then, the backside graphene of the sample was etched by O_2 plasma, and the Cu substrate of supporting Gra was etched with 40% FeCl_3 solution for about 6 h. After, the PMMA/Gra sample was transferred to the target substrate and heated on a hot plate at 85 $^\circ\text{C}$ for 30 min. The PMMA layer was dissolved in acetone (CP) solution at 50 $^\circ\text{C}$ for 10 min, and the target was cleaned with alcohol (EA) solution and deionized (DI) water. Finally, photolithography technology and O_2 plasma etching were used for patterning graphene. The parameters of the O_2 plasma etching were as follows: the power was 60 W, gas flow rate was 30 sccm, and etching time was 3 min. The schematic of transferring the graphene layer to the target substrate is shown in Figure 2.

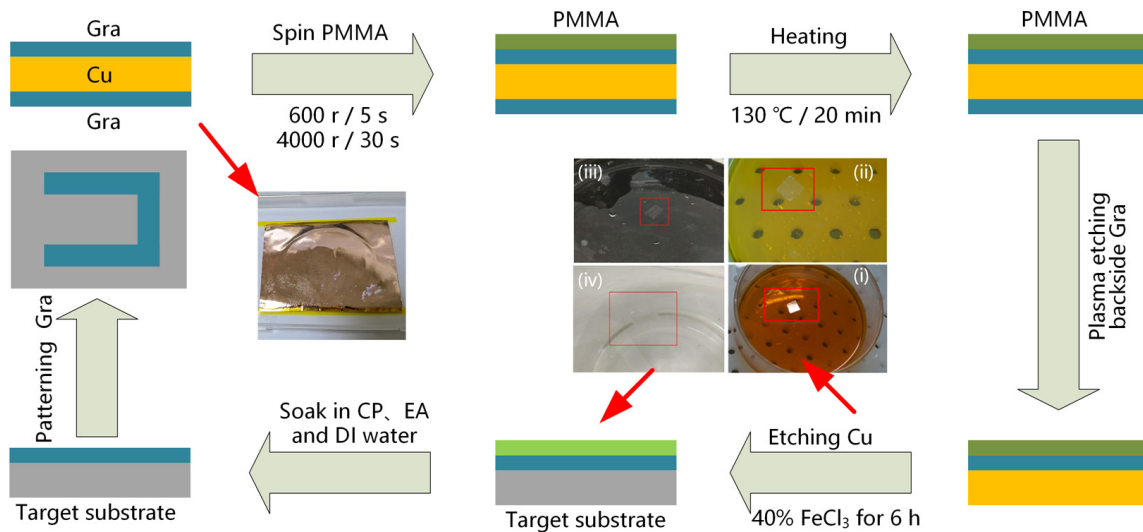


Figure 2. Schematic of transferring graphene layer to target substrate (including patterning graphene).

3. Results and Discussion

3.1. Physical and Electrical Characteristics of the N/MEMS Graphene Units

Raman spectra (HR-800, Horiba Scientific, Inc., Paris, France) were used to analyze the stacking and defects of graphene before and after depositing Si₃N₄. As shown in Figure 3a, the characteristic G and 2D peaks, as well as a weak D peak (defect-related), originating from the CVD-grown monolayer graphene were clearly visible. After depositing the Si₃N₄-protected layer, the intensity of the D peak rapidly increased; meanwhile, the intensity ratio of the 2D peak to the G peak (I_{2D}/I_G) decreased immensely from 3.08 to 0.60. Moreover, a slight shift in the G and 2D peaks was also observed [38,39]. The main explanation for the above phenomena is that the introduction of external atoms disrupts the lattice structure of graphene. Current–voltage (I–V) characteristics were precisely demonstrated by a probing station united with a semiconductor parameter analyzer (B1500A, Keysight, Inc., Santa Rosa, CA, USA). The measurement results are shown in Figure 3b. Compared with the resistance of the open face graphene sensing element from 497.5 to 502.4 $\Omega \cdot \text{sq}^{-1}$, Si₃N₄-encapsulated graphene resistance ranged from 566.1 to 570.8 $\Omega \cdot \text{sq}^{-1}$. This indicated that graphene can retain high quality and consistency after overlaying a Si₃N₄ protective layer.

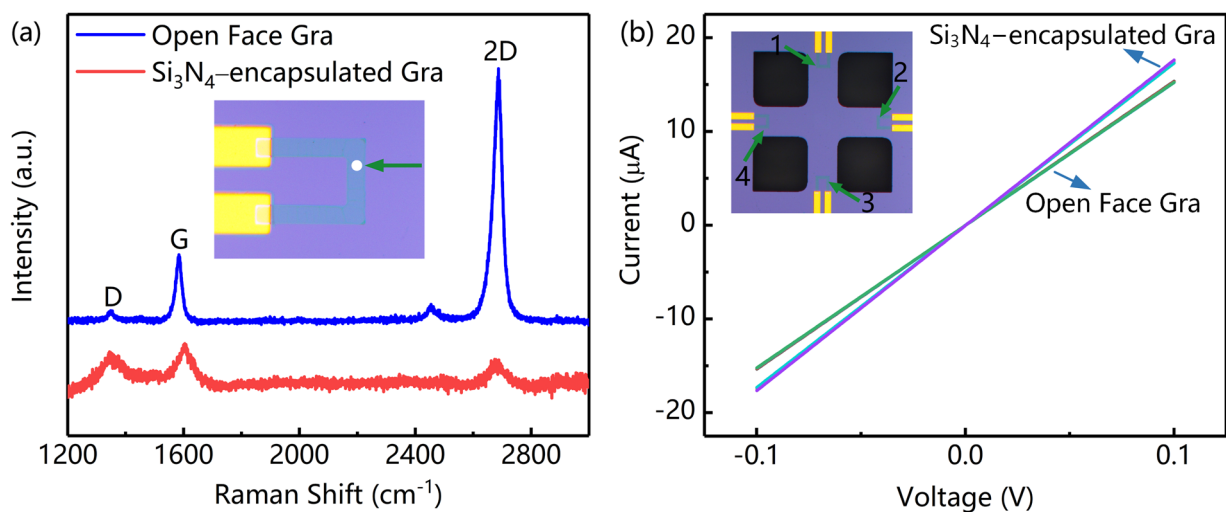


Figure 3. Physical and electrical characteristics of graphene sensing element. (a) Raman spectra of graphene sensing element before and after depositing Si₃N₄. (b) I–V curve of graphene sensing element with open face and Si₃N₄ protective layer.

To further investigate the effect of a Si_3N_4 layer on the stability of the graphene sensing element, samples with and without the top Si_3N_4 layer were placed in ambient air (20~25 °C and relative humidity 40~60%). From Figure 4a, after 7 days, the graphene resistance without top Si_3N_4 increased by $\Delta R/R_0 = 25.8\%$, where R_0 is the initial resistance. In contrast, the relative resistance protected with a Si_3N_4 layer was almost unchanged, showing higher stability. The main reason is that Si_3N_4 can effectively isolate graphene and avoid water or air doping [38]. After 35 days, the unprotected graphene resistance continued to increase, while the protected one remained only slightly increased, as shown in Figure 4b. The corresponding changes in resistance were 7.4% and 46.3%, respectively. We confirmed that the stable performance of graphene resistance is well preserved due to the Si_3N_4 protecting graphene from serious environmental pollution or doping [36].

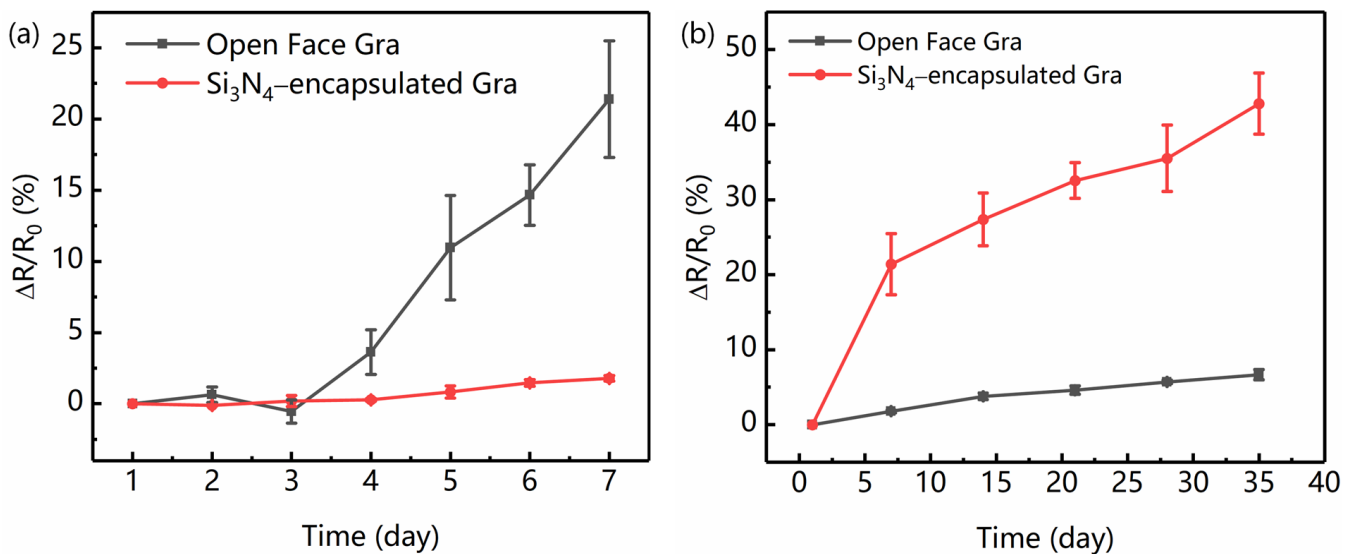


Figure 4. Stability of graphene sensing element with and without the top Si_3N_4 layer: (a) 7 and (b) 35 days later.

3.2. Mechanical and Electrical Characteristics of Displacement Sensor

Tests of the piezoresistive effect for the graphene sensing element on the crossbeam structure were then performed in an uncomplicated experiment. The setup schematic is shown in Figure 5a. There were eight independent sensing units of the same size, distributed on the surface of chip. Four of them were arranged outside the crossbeam as references and did not sense mechanical signals such as strain, on which electrical tests were mainly performed during fabricating to judge the compatibility and reliability of the process. Other graphene sensing units were located at the root of the crossbeam and were utilized to detect the beam strain signal. A piezo actuator with subnanometer resolution (P-841, Physik Instrumente, Inc., Karlsruhe, Germany) was then used to compress the center of the crossbeam. As the actuator simulated external force to produce a tiny displacement, the bend deformation of the crossbeam correspondingly occurred; meanwhile, the graphene sensing element was affected by stress and strain. The resistances of the four graphene varistors were recorded through a digital multimeter (34461A, Keysight Technologies, Inc., Santa Rosa, CA, USA). Measurement results are shown in Figure 5b. After three cycles of the load–unload experiment, with displacement ranging from 0 to 4.5 μm , the changes in resistance and displacement exhibited an apparent positive linear correlation. Moreover, the output results of the four detection units had high consistency, which further verified that the strain generated at the root of the crossbeam remained the same as when the pressure was applied at the center. The piezoresistive effect of graphene is independent of random crystal orientation and multigrain graphene flake [13].

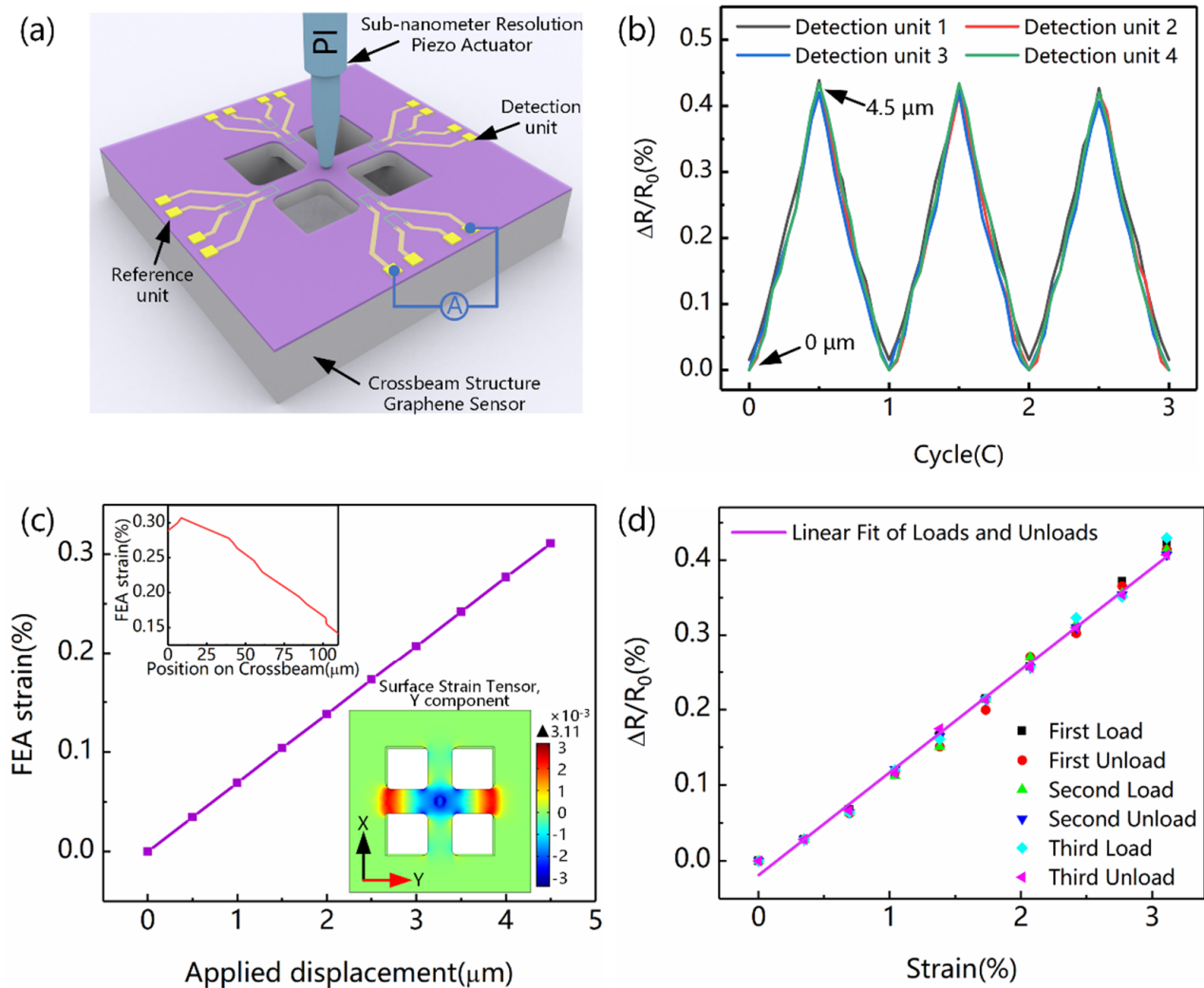


Figure 5. Experimental characterization of crossbeam structure with graphene sensing element. (a) Schematic of experimental setup. (b) Measurement results of displacement resistance. (c) Strain–displacement diagram of crossbeam root by FEA. (d) Strain–resistance results of the detection unit 1.

The piezoresistive effect of the graphene sensing element, through the strain–induced resistance change, was further investigated by finite element analysis (FEA). During FEA simulation, differential displacement load, ranged from 0 to 4.5 μm with a step of 0.5 μm , was applied on the center of the crossbeam structure. Although the maximum displacement was located at the center of the crossbeam, the maximum stress (i.e., strain) appeared at the root of the crossbeam. As shown in Figure 5c, the typical surface maximum strain distribution at the root of a single beam was extracted under different displacements. The internal illustrations showed the strain distribution within the range of 110 μm at the root and the Y component of the surface strain tensor under the applied displacement of 4.5 μm . The X component of the tensor was the same as that of the Y component, and they were perpendicular to one another. We found that the effective strain region was located within 110 μm of the root of the crossbeam. In our work, the graphene sensing element was arranged within 15 μm , which included the position of maximum strain. Because strain was the main factor causing the piezoresistive effect of graphene, the maximum strain parameter was used instead of the displacement parameter. Because the output characteristics of the four detection units were basically similar, only one of them was analyzed in detail. The corresponding result of strain–resistance is shown in Figure 5d. The gauge factor (G) of the graphene piezoresistor was defined as the rate of resistance change to strain ($\Delta R/R_0/\epsilon$). Finally, $G = 1.35$ was obtained in this work, which is similar to the

$G = 1.6$ for CVD graphene obtained in previous research [15]. This also demonstrates the feasibility of arrangement of the graphene sensing element.

3.3. Mechanical and Electrical Characteristics of Pressure Sensor

A new type of graphene pressure sensor was developed by stacking an elastic diaphragm, crossbeam chip, and substrate through bonding technology. Figure 6a shows a schematic diagram of the pressure sensor packaging and actual sensor chip. Furthermore, the chip was assembled on the shell, and the signal was led out by wire bonding. In addition, a wheatstone bridge with a constant current supply was used to detect the electrical conductivity changes in a graphene nanofilm caused by external pressure, as shown in Figure 6b. The pressure sensor was then tested by using a self-made oil pressure calibration machine. Figure 6c shows the voltage output results of 10 cycles in the range of 0~20 MPa, with an interval of 1MPa. The graphene sensing element was not only directly covered by Si_3N_4 , but also isolated from the environment by multistack bonding. Double protection for graphene can greatly improve the repeatability and stability of a sensor. The results of three reciprocating cycles were extracted, as shown in Figure 6d. The calculated sensitivity of the sensor was 33.13 mV/V/MPa. Correspondingly, the hysteresis error, nonlinear error, and repeatability error reached 2.0119%, 3.3622%, and 4.0271%, respectively.

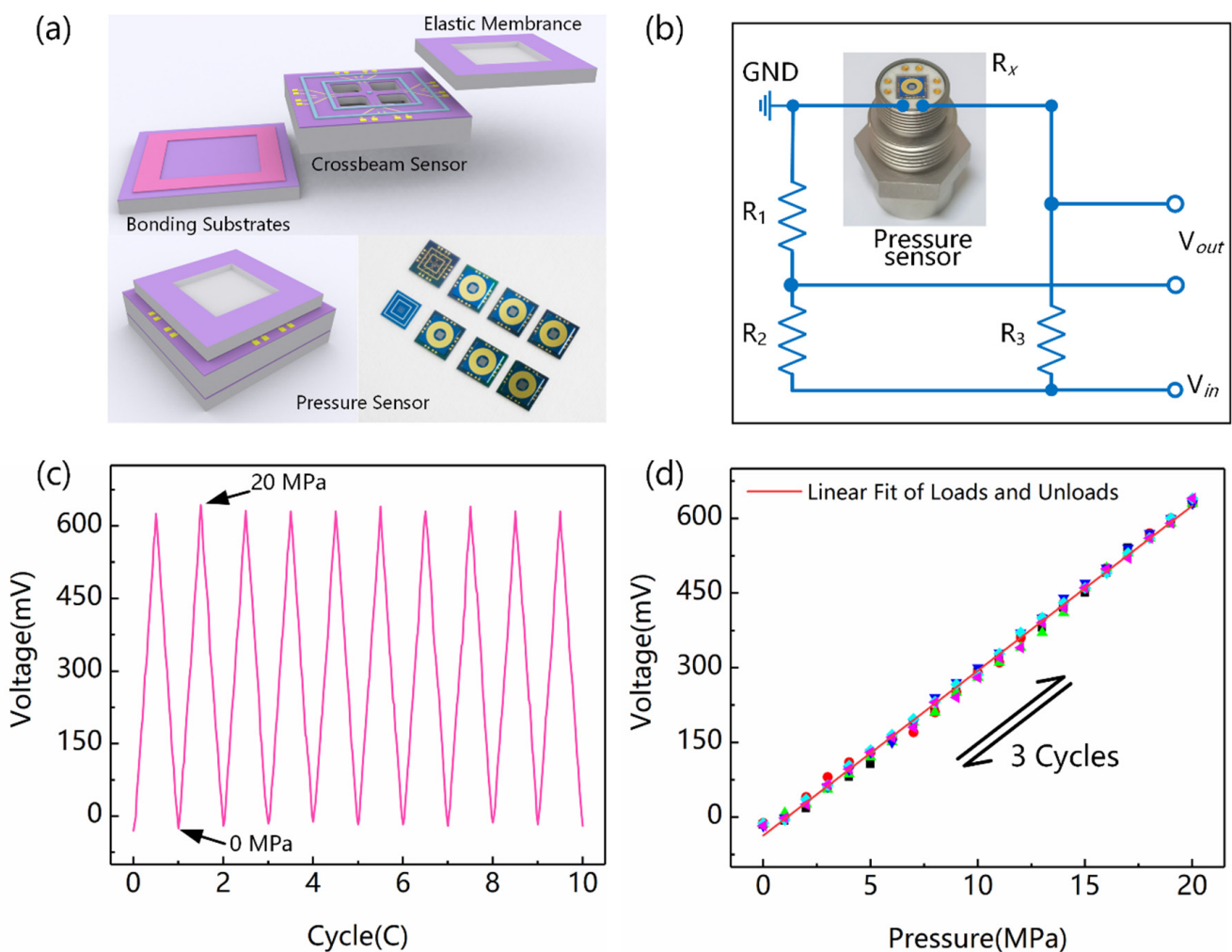


Figure 6. Packaging and testing of graphene pressure sensor based on crossbeam. (a) Packaging schematic and actual chip of sensor. (b) Shell assembling and electrical connection of sensor. (c) Test results of 10 load-unload cycles in full-range condition. (d) Test results of 3 reciprocating cycles.

4. Conclusions

In conclusion, a novel crossbeam structure was employed for graphene N/MEMS mechanical sensors in this work, which significantly overcomes some disadvantages in the performance stability and fabrication process of a suspended structure. Defect free structure and high-quality graphene was demonstrated by a SEM inspection, Raman analysis, and I–V measurement. The results of stability tests further confirmed that Si₃N₄ protection can prolong the working life of graphene devices. The piezoresistive effect of the graphene sensing element was gradually confirmed through displacement resistance measurements and strain–resistance analysis. In the end, a gauge factor of 1.35, near to that of CVD graphene, was reached. Based on the crossbeam structure chip, the sensitivity of the graphene pressure sensor was as high as 33.13 mV/V/MPa under a wide range of conditions. Other static specifications also demonstrated high repeatability and reliability. This indicates that the crossbeam structure is an extremely useful application for graphene N/MEMS mechanical sensors.

Author Contributions: J.W.: conceptualization, methodology, writing—original draft preparation, and project administration; Z.Z.: software and data curation; Y.Q.: validation; M.L.: supervision and funding acquisition. All authors have read and agreed to the published version of the manuscript.

Funding: This research was funded by the “173” Projects of China, grant numbers 2020JCJQZD043, 2021JCJQJJ0172 and 2017JCJQZD006.

Data Availability Statement: Not applicable.

Acknowledgments: The authors are thankful for the facility assistance from the Suzhou Institute of Nano–Tech and Nano–Bionics, Chinese Academy of Sciences.

Conflicts of Interest: The authors declare no conflict of interest.

References

1. Lee, C.; Wei, X.; Kysar, J.W.; Hone, J. Measurement of the elastic properties and intrinsic strength of monolayer graphene. *Science* **2008**, *321*, 385–388. [[CrossRef](#)] [[PubMed](#)]
2. Balandin, A.A.; Ghosh, S.; Bao, W.; Calizo, I.; Teweldebrhan, D.; Miao, F.; Lau, C.N. Superior Thermal Conductivity of Single-Layer Graphene. *Nano Lett.* **2008**, *8*, 902–907. [[CrossRef](#)] [[PubMed](#)]
3. Nair, R.R.; Blake, P.; Grigorenko, A.N.; Novoselov, K.S.; Booth, T.J.; Stauber, T.; Peres, N.M.R.; Geim, A.K. Fine Structure Constant Defines Visual Transparency of Graphene. *Science* **2008**, *320*, 1308. [[CrossRef](#)] [[PubMed](#)]
4. Du, X.; Skachko, I.; Barker, A.; Andrei, E.Y. Approaching ballistic transport in suspended graphene. *Nat. Nanotechnol.* **2008**, *3*, 491–495. [[CrossRef](#)]
5. Ni, Z.; Yu, T.; Lu, Y.H.; Wang, Y.Y.; Feng, Y.P.; Shen, Z.X. Uniaxial Strain on Graphene: Raman Spectroscopy Study and Band-Gap Opening. *ACS Nano* **2008**, *2*, 2301–2305. [[CrossRef](#)]
6. Koenig, S.; Boddeti, N.; Dunn, M.; Bunch, J.S. Ultrastrong adhesion of graphene membranes. *Nat. Nanotechnol.* **2011**, *6*, 543–546. [[CrossRef](#)]
7. Davidovikj, D.; Scheepers, P.H.; Van Der Zant, H.S.J.; Steeneken, P.G.; Davidovikj, D.; Scheepers, P.H.; Van Der Zant, H.S.J.; Steeneken, P.G.; Davidovikj, D.; Scheepers, P.H.; et al. Static Capacitive Pressure Sensing Using a Single Graphene Drum. *ACS Appl. Mater. Interfaces* **2017**, *9*, 43205–43210. [[CrossRef](#)]
8. Wang, Q.; Hong, W.; Dong, L. Graphene “microdrums” on a freestanding perforated thin membrane for high sensitivity MEMS pressure sensors. *Nanoscale* **2016**, *8*, 7663–7671. [[CrossRef](#)]
9. Chen, H.; Lv, L.; Zhang, J.; Zhang, S.; Xu, P.; Li, C.; Zhang, Z.; Li, Y.; Xu, Y.; Wang, J. Enhanced Stretchable and Sensitive Strain Sensor via Controlled Strain Distribution. *Nanomaterials* **2020**, *10*, 218. [[CrossRef](#)]
10. Fan, X.; Forsberg, F.; Smith, A.D.; Schröder, S.; Wagner, S.; Östling, M.; Lemme, M.C.; Niklaus, F. Suspended Graphene Membranes with Attached Silicon Proof Masses as Piezoresistive Nanoelectromechanical Systems Accelerometers. *Nano Lett.* **2019**, *19*, 6788–6799. [[CrossRef](#)]
11. Wu, S.; Peng, S.; Han, Z.J.; Zhu, H.; Wang, C.H. Ultrasensitive and Stretchable Strain Sensors Based on Mazelike Vertical Graphene Network. *ACS Appl. Mater. Interfaces* **2018**, *10*, 36312–36322. [[CrossRef](#)] [[PubMed](#)]
12. Bae, S.-H.; Lee, Y.; Sharma, B.K.; Lee, H.-J.; Kim, J.-H.; Ahn, J.-H. Graphene-based transparent strain sensor. *Carbon* **2013**, *51*, 236–242. [[CrossRef](#)]
13. Smith, A.D.; Niklaus, F.; Paussa, A.; Vaziri, S.; Fischer, A.C.; Sterner, M.; Forsberg, F.; Delin, A.; Esseni, D.; Palestri, P.; et al. Electromechanical Piezoresistive Sensing in Suspended Graphene Membranes. *Nano Lett.* **2013**, *13*, 3237–3242. [[CrossRef](#)] [[PubMed](#)]

14. Smith, A.; Vaziri, S.; Niklaus, F.; Fischer, A.; Sterner, M.; Delin, A.; Östling, M.; Lemme, M. Pressure sensors based on suspended graphene membranes. *Solid-State Electron.* **2013**, *88*, 89–94. [[CrossRef](#)]
15. Zhu, S.-E.; Ghatkesar, M.K.; Zhang, C.; Janssen, G.C.A.M. Graphene based piezoresistive pressure sensor. *Appl. Phys. Lett.* **2013**, *102*, 161904. [[CrossRef](#)]
16. Hurst, A.M.; Lee, S.; Cha, W.; Hone, J. A graphene accelerometer. In Proceedings of the 2015 28th IEEE International Conference on Micro Electro Mechanical Systems (MEMS), Estoril, Portugal, 18–22 January 2015; pp. 865–868. [[CrossRef](#)]
17. Fan, X.; Smith, A.D.; Forsberg, F.; Wagner, S.; Schröder, S.; Akbari, S.S.A.; Fischer, A.C.; Villanueva, L.G.; Östling, M.; Lemme, M.C.; et al. Manufacture and characterization of graphene membranes with suspended silicon proof masses for MEMS and NEMS applications. *Microsyst. Nanoeng.* **2020**, *6*, 17. [[CrossRef](#)]
18. Park, W.-T.; Kotlanka, R.K.; Lou, L.; Hamidullah, M.; Lee, C. MEMS tri-axial force sensor with an integrated mechanical stopper for guidewire applications. *Microsyst. Technol.* **2012**, *19*, 1005–1015. [[CrossRef](#)]
19. Chun, S.; Choi, Y.; Park, W. All-graphene strain sensor on soft substrate. *Carbon* **2017**, *116*, 753–759. [[CrossRef](#)]
20. Zhang, Z.; Du, J.; Zhang, D.; Sun, H.; Yin, L.; Ma, L.; Chen, J.; Ma, D.; Cheng, H.-M.; Ren, W. Rosin-enabled ultraclean and damage-free transfer of graphene for large-area flexible organic light-emitting diodes. *Nat. Commun.* **2017**, *8*, 14560. [[CrossRef](#)]
21. Liang, X.; Sperling, B.A.; Calizo, I.; Cheng, G.; Hacker, C.; Zhang, Q.; Obeng, Y.; Yan, K.; Peng, H.; Li, Q.; et al. Toward Clean and Crackless Transfer of Graphene. *ACS Nano* **2011**, *5*, 9144–9153. [[CrossRef](#)]
22. Suk, J.W.; Lee, W.H.; Lee, J.; Chou, H.; Piner, R.D.; Hao, Y.; Akinwande, D.; Ruoff, R.S. Enhancement of the Electrical Properties of Graphene Grown by Chemical Vapor Deposition via Controlling the Effects of Polymer Residue. *Nano Lett.* **2013**, *13*, 1462–1467. [[CrossRef](#)] [[PubMed](#)]
23. Ahn, Y.; Kim, H.; Kim, Y.-H.; Yi, Y.; Kim, S.-I. Procedure of removing polymer residues and its influences on electronic and structural characteristics of graphene. *Appl. Phys. Lett.* **2013**, *102*, 091602. [[CrossRef](#)]
24. Piazza, A.; Giannazzo, F.; Buscarino, G.; Fisichella, G.; La Magna, A.; Roccaforte, F.; Cannas, M.; Gelardi, F.; Agnello, S. Graphene p-Type Doping and Stability by Thermal Treatments in Molecular Oxygen Controlled Atmosphere. *J. Phys. Chem. C* **2015**, *119*, 22718–22723. [[CrossRef](#)]
25. Russo, S.; Craciun, M.; Yamamoto, M.; Morpurgo, A.; Tarucha, S. Contact resistance in graphene-based devices. *Phys. E Low-Dimens. Syst. Nanostruct.* **2009**, *42*, 677–679. [[CrossRef](#)]
26. Li, M.; Wu, C.; Zhao, S.; Deng, T.; Wang, J.; Liu, Z.; Wang, L.; Wang, G. Pressure sensing element based on the BN-graphene-BN heterostructure. *Appl. Phys. Lett.* **2018**, *112*, 143502. [[CrossRef](#)]
27. Al-Mumen, H.; Dong, L.; Li, W. SU-8 doped and encapsulated n-type graphene nanomesh with high air stability. *Appl. Phys. Lett.* **2013**, *103*, 232113. [[CrossRef](#)]
28. Seo, H.-K.; Park, M.-H.; Kim, Y.-H.; Kwon, S.-J.; Jeong, S.-H.; Lee, T.-W. Laminated Graphene Films for Flexible Transparent Thin Film Encapsulation. *ACS Appl. Mater. Interfaces* **2016**, *8*, 14725–14731. [[CrossRef](#)]
29. Jee, H.-G.; Han, J.-H.; Hwang, H.-N.; Kim, B.; Kim, H.-S.; Kim, Y.D.; Hwang, C.-C. Pentacene as protection layers of graphene on SiC surfaces. *Appl. Phys. Lett.* **2009**, *95*, 093107. [[CrossRef](#)]
30. Alexandrou, K.; Petrone, N.; Hone, J.; Kymissis, I. Encapsulated graphene field-effect transistors for air stable operation. *Appl. Phys. Lett.* **2015**, *106*, 113104. [[CrossRef](#)]
31. Wang, H.; Taychatanapat, T.; Hsu, A.; Watanabe, K.; Taniguchi, T.; Jarillo-Herrero, P.; Palacios, T. BN/Graphene/BN Transistors for RF Applications. *IEEE Electron. Device Lett.* **2011**, *32*, 1209–1211. [[CrossRef](#)]
32. Jain, N.; Durcan, C.A.; Jacobs-Gedrim, R.; Xu, Y.; Yu, B. Graphene interconnects fully encapsulated in layered insulator hexagonal boron nitride. *Nanotechnology* **2013**, *24*, 355202. [[CrossRef](#)] [[PubMed](#)]
33. Yang, M.; Zhang, C.; Wang, S.; Feng, Y. Ariando Graphene on β -Si₃N₄: An ideal system for graphene-based electronics. *AIP Adv.* **2011**, *1*, 032111. [[CrossRef](#)]
34. Fan, Y.; Jiang, W.; Kawasaki, A. Highly Conductive Few-Layer Graphene/Al₂O₃Nanocomposites with Tunable Charge Carrier Type. *Adv. Funct. Mater.* **2012**, *22*, 3882–3889. [[CrossRef](#)]
35. Lee, J.; Tao, L.; Parrish, K.N.; Hao, Y.; Ruoff, R.S.; Akinwande, D. Multi-finger flexible graphene field effect transistors with high bendability. *Appl. Phys. Lett.* **2012**, *101*, 252109. [[CrossRef](#)]
36. Yap, R.C.C.; Li, H.; Chow, W.L.; Lu, C.X.; Tay, B.K.; Teo, H.T.E. Identifying the mechanisms of p-to-n conversion in unipolar graphene field-effect transistors. *Nanotechnology* **2013**, *24*, 195202. [[CrossRef](#)]
37. Wang, Z.; Li, P.; Chen, Y.; Liu, J.; Qi, F.; Tian, H.; Zheng, B.; Zhou, J. Air-stable n-type doping of graphene from overlying Si₃N₄ film. *Appl. Surf. Sci.* **2014**, *307*, 712–715. [[CrossRef](#)]
38. Geng, D.; Yang, S.; Zhang, Y.; Yang, J.; Liu, J.; Li, R.; Sham, T.-K.; Sun, X.; Ye, S.; Knights, S. Nitrogen doping effects on the structure of graphene. *Appl. Surf. Sci.* **2011**, *257*, 9193–9198. [[CrossRef](#)]
39. Su, F.; Zhang, Z.; Li, S.; Li, P.; Deng, T. Long-term stability of photodetectors based on graphene field-effect transistors encapsulated with Si₃N₄ layers. *Appl. Surf. Sci.* **2018**, *459*, 164–170. [[CrossRef](#)]